



HAL
open science

Experimental evidence of settling retardation in a turbulence column

Yulia Akutina, Thibaud Revil-Baudard, Julien Chauchat, Olivier Eiff

► **To cite this version:**

Yulia Akutina, Thibaud Revil-Baudard, Julien Chauchat, Olivier Eiff. Experimental evidence of settling retardation in a turbulence column. *Physical Review Fluids*, 2020, 5 (1), 10.1103/PhysRevFluids.5.014303 . hal-02441548

HAL Id: hal-02441548


<https://hal.science/hal-02441548v1>

Submitted on 1 Nov 2024

HAL is a multi-disciplinary open access archive for the deposit and dissemination of scientific research documents, whether they are published or not. The documents may come from teaching and research institutions in France or abroad, or from public or private research centers.

L'archive ouverte pluridisciplinaire **HAL**, est destinée au dépôt et à la diffusion de documents scientifiques de niveau recherche, publiés ou non, émanant des établissements d'enseignement et de recherche français ou étrangers, des laboratoires publics ou privés.

Experimental evidence of settling retardation in a turbulence column

Y. Akutina ^{1,*} T. Revil-Baudard,^{1,2} J. Chauchat,² and O. Eiff¹

¹*Institute for Hydromechanics, Karlsruhe Institute of Technology, Kaiserstrasse 12,
D-76131 Karlsruhe, Germany*

²*LEGI, Grenoble University, Domaine Universitaire, BP 53, F-38041 Grenoble Cedex 9, France*

Settling experiments were conducted in a turbulence column to investigate the effect of turbulence on the effective fall velocity of solid particles slightly denser than the fluid ($\rho_p \gtrsim \rho_f$). Five types of particles of different materials and shapes were tested, their size ranging between $o(1)\eta$ and $o(10)\eta$, where η is the Kolmogorov viscous length scale. Thus, the particles were of finite size with an unknown analytical form for the fluid-particle forces. The density ratio ranged as $(\rho_p - \rho_f)/\rho_f = \{0.13 : 1.6\}$, and the still-fluid particle Reynolds number as $\text{Re}_p^0 = \{75 : 981\}$. The turbulence levels characterized with the integral-scale Reynolds number ranged as $\text{Re}_L = \{34 : 510\}$. Two-dimensional (2D) particle image velocimetry was used to obtain flow statistics, the residual mean circulation, and the turbulence statistics, while 2D particle tracking was performed to measure particle settling velocities. For all types of particles tested, settling retardation is observed as the turbulence intensity is increased. It is found that if both the effective fall velocity W_s and the turbulent fluid velocity $W_{f,\text{rms}}$ are nondimensionalized by the still-fluid particle terminal velocity W_0 , the settling retardation can be described by a unique relation independent of the particle type, $W_s/W_0 = f(W_{f,\text{rms}}/W_0)$, for the given range of flow regimes. Using analytical descriptions of the loitering and nonlinear drag effects, this scaling is shown to have a solid physical basis.

I. INTRODUCTION

An accurate prediction of the effective fall velocity of solid particles settling in a turbulent fluid is of major importance for a large number of industrial and geophysical applications [1–3]. It is a critical parameter in the dispersion models used to predict the spatial and temporal distribution of solid particles in turbulent flows [4–6]. It has been shown that the particle fall velocity can be either enhanced or hindered by the fluid turbulence [7–10]. Four main mechanisms have been identified to explain the turbulence-induced modification of the effective fall velocity (i.e., the settling velocity). First, the *fast-tracking effect* tends to increase the fall velocity due to the preferential sampling of downward-moving fluid regions. It appears to be caused by an inertial bias in the trajectory of very heavy particles ($\rho_p \gg \rho_f$) of the same order in size or smaller than the dissipation scales ($d_p \lesssim \eta$ [9]). The *fast-tracking effect* occurs, for instance, in the case of liquid droplets settling in a turbulent gas (e.g., Ref. [11]). The three remaining mechanisms induce a settling retardation. The *vortex trapping* concerns small and light particles ($d_p \lesssim \eta$ and $\rho_p \approx \rho_f$). It occurs when the turbulent velocity is greater than the still-fluid terminal fall velocity $W_{f,\text{rms}} > W_0$ [7]. The *loitering effect* is induced by the difference in the time periods spent by the particle to traverse upward and downward fluid velocity regions [12]. As it takes longer to traverse an upward-moving fluid zone

*yulia.akutina@kit.edu

than a downward-moving one, the averaged velocity is biased towards lower values and the fall velocity is reduced on average. Yet, the favorable conditions for the loitering effect to occur are still not well characterized. The third mechanism decelerating particle settling is the *nonlinear drag effect*. When the particulate Reynolds number ($\text{Re}_p^0 = d_p W_0 / \nu$) is greater than unity, the relation between the drag force exerted by the fluid on the particle F_D and the relative velocity V is such that $F_D \propto V^\beta$, with $1 < \beta \leq 2$ [13,14]. When the relative velocity between the fluid and the particle fluctuates in time, the nonlinearity induces a positive drag force increment, leading to a reduction of the settling velocity [8,15].

It was observed that when the particles are heavy ($\rho_p \gg \rho_f$) and small ($d_p \lesssim \eta$) the fast-tracking effect appears to dominate, leading to enhanced fall velocities (e.g., Refs. [4,9,16,17]). Falling retardation, on the other hand, is predominantly observed for particles slightly denser than the fluid ($\rho_p / \rho_f \gtrsim 1$) when the fast-tracking effect induced by the particle inertia is less important. However, there is a lack of consensus about the interplay and even the existence of some of the four interaction mechanisms [11,18,19]. For instance, the effective influence of nonlinear drag and loitering is still controversial. The numerical simulations presented in Ref. [11] suggest that the retardation is imputable to nonlinear drag. On the other hand, the numerical results of Ref. [18] show that the loitering effect dominates the settling retardation and that nonlinear drag can be neglected [12]. This lack of agreement results partly from the lack of controlled experiments involving large solid particles ($\text{Re}_p^0 \gg 1$) settling in a dense turbulent fluid ($\rho_p / \rho_f \gtrsim 1$). First, the majority of the experimental and numerical studies have focused on small particles for which the linear Stokes drag law holds ($\text{Re}_p^0 \lesssim 1$). Second, the pioneering experiments (e.g., Ref. [20]) in which larger particles were considered could not rigorously account for the mean-flow patterns which are difficult to avoid when generating homogeneous turbulence from oscillating grids. The intensity of these mean fluid motions can be of the order of the particle settling velocity and therefore strongly affects the measurements. For instance, Ref. [21] performed experiments based on two-phase optical measurements. To correct for the mean currents in the turbulence column, the fluid velocities averaged over (a rather small) measurement area and over a short period of time were subtracted from the settling velocities. This method of accounting for the mean currents may not be optimal since the motion of large-scale turbulent structures may be subtracted as well. Nevertheless, the authors obtained that on average the relative velocity of the particle was smaller than the settling velocity in still water. An analytical model based on the loitering effect allowed a partial explanation of the results.

In this paper, we aim at obtaining particle settling data in a turbulence column for a relatively wide range of particle properties and turbulent intensities, while carefully accounting for the mean-flow patterns. The rest of the paper is structured as follows. The experimental methodology is presented in Sec. II. Experimental results that include the turbulence properties in the oscillating-grid facility and particles settling velocities are given in Sec. III. Theoretical considerations on nonlinear drag and loitering effects are presented in Sec. IV. Conclusions (Sec. V) are given in the end.

II. EXPERIMENTAL PROCEDURE

In this section, the measurement methodology of the particle fall velocities in a turbulence column and of the measurements of the associated ambient turbulence is presented.

A. Turbulence column

Settling experiments were performed in the turbulence column situated in the Institute for Hydromechanics in Karlsruhe Institute of Technology. This facility was designed by Ref. [22] on the basis of the apparatus presented in Ref. [23]. It consists of a glass reservoir 50 cm wide, 35 cm deep, and 133 cm high, inside of which five pairs of grids facing each other are installed along the two vertical walls (Fig. 1). The size of each grid is 23 cm \times 34 cm with square openings 3.5 cm wide

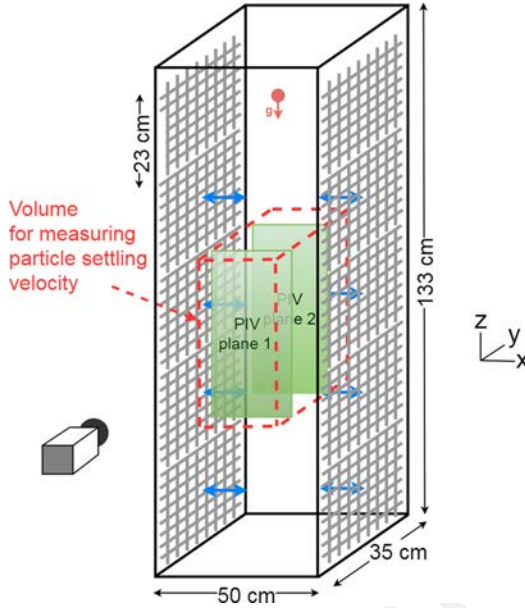


FIG. 1. Sketch of the turbulence column. The dashed red parallelepiped corresponds to the measurement volume, where the settling of a solid particle was tracked. The two green rectangles correspond to the two planes where fluid velocity measurements were performed using PIV. Both sides of the tank are equipped with five grids each, all oscillating independently at random phase. The top two are not activated in this study. The blue arrows show the direction of the grids' oscillation.

with 1-cm-thick square bars in between, resulting in 40% blockage. The grids can be oscillated horizontally at independent frequencies and amplitudes. In the present experiments, all the grids oscillated with the same amplitude and frequency while being out of phase, i.e., each of the eight of them was in its own phase defined randomly. (The top pair of grids was not activated to avoid free-surface disturbances.) The oscillation amplitude was kept at 3 cm while the frequency was varied in the range $F \in [1 : 9]$ Hz by steps of 2 Hz for different experimental runs.

B. Fluid velocity measurements

The fields of instantaneous horizontal (u) and vertical (w) fluid velocities are measured using two-dimensional (2D) particle image velocimetry (PIV). The working fluid (water) is seeded with small ($50\text{-}\mu\text{m}$) neutrally buoyant (density of 1.03 g/cm^3) noninertial (Stokes number < 0.01) polyamid particles. The seeding particles are illuminated from above the tank with a 3-mm-thick laser sheet generated by a continuous 2-W solid-state laser. Image pairs are acquired at the frequency of 0.99 Hz using an 8-bit complementary metal-oxide semiconductor (CMOS) camera with a resolution of 1936×1216 pixels. The time interval between two consecutive images used to derive the velocity vectors lies between 7 and 30 ms for the lowest and highest stirring frequencies, respectively.

The camera is positioned on the side of the tank and takes images of the vertical laser planes through the Plexiglas wall (Fig. 1). The measurement field is $18\text{ cm} \times 27\text{ cm}$ (x, z) and is orthogonal to the grids' plane (y, z). It is located 50 cm below the free surface and is centered between the grids. The experiments are repeated in two parallel planes with an offset of 18 cm in the O_y direction.

The images are processed with a direct correlation method based on Refs. [24,25]. The spatial resolution based on the size of the correlation box (20×20 pixels) is 3 mm. Velocity vectors are computed on a grid with a spacing of 10 pixels (i.e., 50% overlap). For each stirring frequency

and each y plane, $N = 500$ velocity measurements were performed to obtain the mean horizontal, $\overline{U}(x, z)$, and vertical, $\overline{W}(x, z)$, fluid velocities and the turbulence intensities, $U_{f,\text{rms}}(x, z) = \sqrt{\overline{u'^2(x, z)}}$ and $W_{f,\text{rms}}(x, z) = \sqrt{\overline{w'^2(x, z)}}$, where $u'(x, z)$ and $w'(x, z)$ are the fluid velocity fluctuations and the overbar denotes time averaging.

In order to verify the statistical homogeneity of the flow in the transverse direction Oy , the measurements in the two y planes were compared. Since the mean velocity in the turbulence column is approximately zero it is not reasonable to compare the difference between the two planes with the (small) residual of the mean velocity. Instead, comparing it with the particle settling velocity is more appropriate. It is found that over the entire frequency range, the absolute difference in the mean flow between the two planes is less than 10% of the lowest still-water particle settling velocity W_0 . The difference in the turbulence intensities is also lower than 10%. Since these differences are sufficiently small for the following scaling analysis, the flow can be considered uniform in the y direction. Thus, the mean flow and turbulent intensities are averaged between the two planes.

C. Particle velocity measurements

The solid particles are manually released into the tank from the top and center, one at a time. As a particle settles through the turbulence column, its trajectory is recorded, and its instantaneous velocities are calculated. When it reaches the bottom of the tank, the next particle is released. The tank is illuminated with white light and the same camera, used for the PIV measurements (at the same position), is used to record the particles' trajectories projected on the x - z plane (Fig. 1). Given that the flow statistics are homogeneous in the y direction (see Sec. II B), planar measurements are justified. The images are acquired at a frequency of 10 Hz. The particle image size ranges from about 15 to 35 pixels and their centroids are determined after applying an intensity criteria to filter out background noise. Subtracting the position of the particles between two consecutive images yields the horizontal and vertical displacements (Δx and Δz , respectively). Dividing the horizontal and vertical displacements by the time step between consecutive images yields horizontal, u'_s , and vertical, w'_s , velocities, respectively. A first-order scheme is used herein given that the turbulence intensity is relatively weak. The measurement volume is chosen such that each particle reaches its terminal velocity in still water (W_0) before entering it. This was verified by measuring the settling velocities above it. On average, the particles accelerated until $z \approx 25$ cm. The measurement area was then chosen to start at $z = 20$ cm (see Fig. 2).

It is inevitable that a mean-flow circulation develops in a closed tank with oscillating grids. While it is possible to make it weak, it is not possible to eliminate it completely. The remaining circulation introduces a bias in the particle settling measurements. In order to eliminate this bias, the local mean fluid velocities due to this circulation, $\overline{U}(x, z)$ and $\overline{W}(x, z)$, obtained from the two-plane averaged PIV measurements, are subtracted from the raw instantaneous particle velocities. This yields the corrected particle velocities $u_s(x, z) = u'_s(x, z) - \overline{U}(x, z)$ and $w_s(x, z) = w'_s(x, z) - \overline{W}(x, z)$. The mean fluid velocities used for the particle velocity correction are the ones measured at the closest location to the particle position (x, z) . This position is also used to relate the fluid turbulence intensities to the particle velocity later on. It is implicitly assumed here that the particles do not affect the mean-flow field.

D. Particle properties

Five different types of particles, S1–S5, are used in the current experiments (Table I). Three of them have a density close to that of the fluid ($\rho_p/\rho_f \approx 1.2$) while the two remaining ones have higher densities ($\rho_p/\rho_f = 1.49$ and 2.6). Their median diameter¹ d_p is between 1.5 and 4.7 mm. The measured still-water settling velocity W_0 ranges from 5.0 to 22.3 cm/s. The particles were

¹The size ranges, given by the \pm sign in Table I, are obtained by measuring the sizes in a sample of particles.

TABLE I. The properties of the settling particles: the particle size d_p (for spherical particles this size corresponds to the diameter, for the cubic one it corresponds to the cubes' side); the particle density ρ_p ; the submerged specific gravity $\frac{\rho_p - \rho_f}{\rho_f}$; the still-water terminal settling velocity W_0 ; the rms of the particle vertical velocity in still water $W_{0,\text{rms}}$; the rms of the particle horizontal velocity in still water $U_{0,\text{rms}}$; the particulate Reynolds number $\text{Re}_p^0 = d_p W_0 / \nu$, where ν is the kinematic viscosity; the ratio between the particle size and the integral length scale of turbulence d_p/L ; and the relaxation time $\tau_p = \frac{2\rho_p/\rho_f + 1}{36} \frac{d_p^2}{\nu} \frac{1}{\Phi(\text{Re}_p^0)}$ [26], where $\Phi(\text{Re}_p^0) = 1 + 0.15(\text{Re}_p^0)^{0.687}$.

Particle	d_p (mm)	ρ_p (kg/m ³)	$\frac{\rho_p - \rho_f}{\rho_f}$	W_0 (cm/s)	$\frac{W_{0,\text{rms}}}{W_0}$ (%)	$\frac{U_{0,\text{rms}}}{W_0}$ (%)	Re_p^0	$\frac{d_p}{L}$	τ_p (s)	Description
S1	1.5 ± 0.05	1130	0.13	5.0	3.8	8	75	0.09	0.05	Plastic cubes
S2	3 ± 0.5	1190	0.19	6.2	21	22	186	0.18	0.13	Plastic, angular shape
S3	4 ± 0.05	1200	0.2	12.9	3.9	6	516	0.23	0.13	Plastic spherical beads
S4	1.8 ± 0.4	1490	0.49	8.3	11	11	141	0.10	0.07	Plastic sand
S5	4.4 ± 0.4	2600	1.6	22.3	16	13	981	0.26	0.19	Natural sand

chosen to cover a range of different shapes. S1 particles are plastic cubes. S2 is made from crushed plexiglass [polymethylmethacrylate (PMMA)], and therefore has an angular irregular form with sharp edges. (These particles were also used in Refs. [27,28].) S3 are spherical plastic beads. S4 are made of plastic but have a shape close to that of sand grains. Particles S5 is natural sand. The dispersion in size and shape between individual particles within one particle type is given by the standard deviation of the still-water terminal velocity $W_{0,\text{rms}}$ (assuming negligible variation of the material density). It can be seen in Table I that S1 and S3 are well sorted, $W_{0,\text{rms}}/W_0 \approx 4\%$, while S2, S4, and S5 have a wider distribution of size and shape, $10\% \lesssim W_{0,\text{rms}}/W_0 \lesssim 20\%$.

E. Measurement uncertainties

The accuracy of fluid velocity measurements via PIV is estimated to be about 0.05 pixels since the peak-locking bias has effectively been removed [24]. For an average displacement of about 10 pixels, the resulting uncertainty of the fluid fluctuations is therefore less than 1%. The uncertainty of the mean (time-averaged) fluid velocities due to the lack of temporal convergence can be calculated by dividing the data set temporally in half and comparing the time averages. The differences throughout the flow field are found to be about 0.1 and 1.3 mm/s for the smallest and highest stirring frequencies, respectively. In relative terms, this translates into about 0.04%–2.6% of W_0 . (Again, the errors in the mean flow cannot be compared with mean values themselves since zero-mean flow is considered herein.) The turbulence intensities are estimated to be converged within about 3%.

The main contributor to the instantaneous particle velocity measurement uncertainty is the error associated with the detection of the particle's centroids. While for spherical particles the image centroid coincides with the mass centroid, for angular-shaped particles there can be an apparent shift of approximately $d_p/4$ due to nonuniform lighting, resulting in an uncertainty of the particle velocity of $d_p/(2\Delta t)$, where $\Delta t = 0.1$ s. However, this error is effectively random and if the data are well converged, it does not have an effect on the time-averaged statistics. The uncertainty in the convergence of the particle velocity measurements ranges between 0.5 and 5 mm/s, corresponding to about 0.25%–1% of W_0 for the lowest stirring frequency, and 2.5%–10% of W_0 at the highest one. Even if these uncertainties do not allow a highly accurate quantitative description, it is considered to be sufficient for the following analysis.

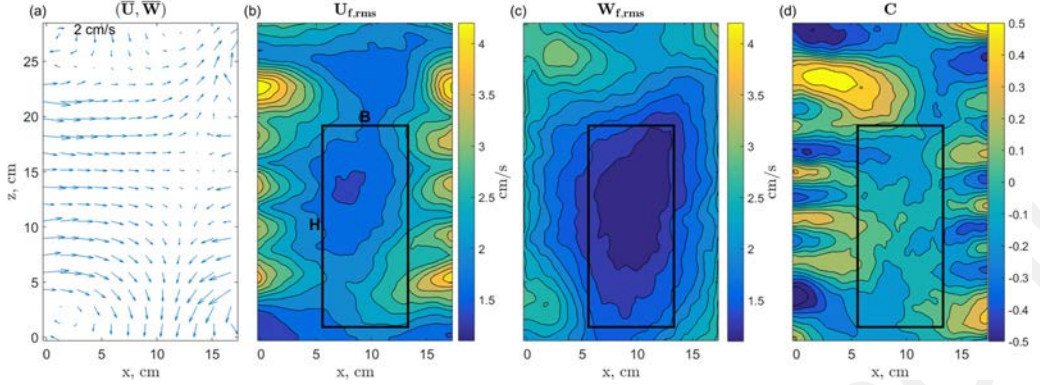


FIG. 2. PIV results for the stirring frequency $F = 5$ Hz. (a) The time-averaged velocity vector field (\bar{U}, \bar{W}) , with the velocity scale given at the top of the plot. (b) The horizontal turbulence intensity $U_{f,rms}$. (c) The vertical turbulence intensity $W_{f,rms}$. (d) The local turbulent correlation coefficient C . The black rectangle represents the region used for the settling velocity analysis (size $B \times H$).

III. RESULTS

A. Turbulence properties

An example of the PIV results for the grid stirring frequency of 5 Hz is given in Figs. 2(a)–2(d). Note that all the flow statistics are averaged over two measurement planes at two y positions, the difference between which is considered to be small (see Sec. II B). For different stirring frequencies the flow patterns are almost identical. Thus, here we present only one stirring frequency as an example. Figure 2(a) shows the time-averaged velocity-vector field, from which it is clear that a mean current of a few cm/s exists in the turbulence column. The horizontal velocity component appears to be asymmetric and more significant than the vertical one. As discussed above (Sec. II C), these local time-averaged flow velocities were subtracted from the horizontal and vertical particle velocities in order to eliminate the bias on the particle settling velocities.

Figures 2(b) and 2(c) show the horizontal, U'_f , and vertical, W'_f , turbulence intensities, respectively. It is clear that closer to the grids (left and right sides of the plots) the horizontal turbulence component is considerably larger than the vertical one. This is to be expected since the grids are oscillating in the horizontal direction. However, towards the center of the tank, the pressure fluctuations redistribute the turbulent kinetic energy (TKE) to the perpendicular components. Yet, even at the center of the tank the turbulence anisotropy does not vanish completely. For the subsequent analysis, the anisotropy is accounted for by considering the vertical and horizontal turbulence intensities separately.

Finally, the turbulent correlation coefficient is presented in Fig. 2(d),

$$C(x, z) = \frac{\overline{u'w'}}{U_{f,rms}W_{f,rms}}, \quad (1)$$

which allows one to assess the importance of the turbulence production due to the shear in the mean flow. In turbulent boundary layers (with high mean shear), its value is considered universal, $C \approx 0.45$ [29,30]. In an idealized statistically homogeneous isotropic turbulence with no mean shear, it should be zero. As the present work aims to study ideally the effect of homogeneous and isotropic turbulence on the particle settling velocity, the region of low correlation coefficient is chosen for the analysis, $C < 0.1$, for all experiments. It is shown as a black rectangle in Figs. 2(b)–2(d). Within this region, the turbulence properties will now be characterized.

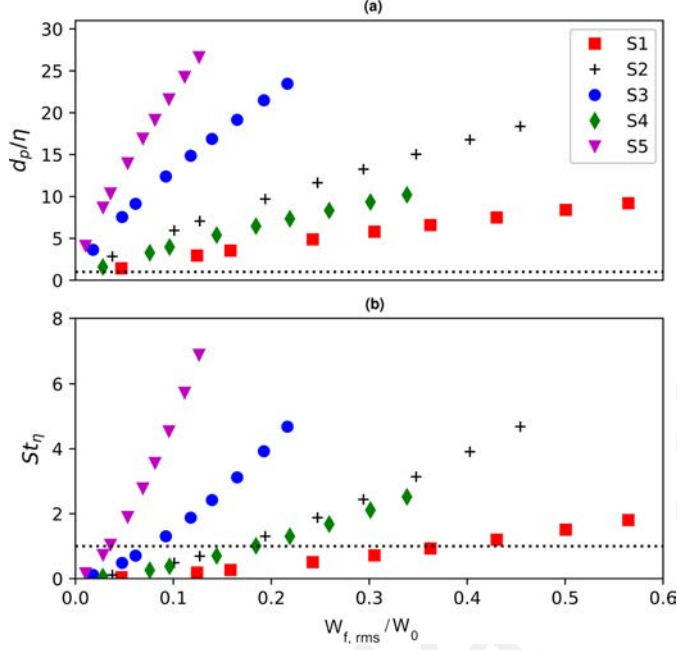


FIG. 3. (a) The ratio between the particle size and dissipation scale, d_p/η , and (b) the particle Stokes number, $St_\eta = \tau_p/\tau_\eta$, as a function of the local dimensionless vertical turbulence intensity, $W_{f,rms}/W_0$, for particle types S1–S5. The dashed lines correspond to $d_p/\eta = 1$ and $St_\eta = 1$.

The turbulent integral length scale L is calculated using the horizontal cross correlation of the vertical velocity fluctuations averaged in the vertical direction,

$$L = \int_{-B/2}^{B/2} \frac{\langle w'(x_1, z)w'(x_1 + x, z) \rangle_z}{W_f^2} dx, \quad (2)$$

where B is the width of the field of view in the horizontal direction [see Fig. 2(b)], and x_1 is its center. For every experiment, the result of this calculation is approximately the same, $L \approx 1.7$ cm, and corresponds to half the mesh size of the oscillating grids, consistent with the results of Ref. [31].

The turbulence intensity varies in the range of $0.2 \text{ cm/s} < W_{f,rms} < 3 \text{ cm/s}$ for the different stirring frequencies investigated. It follows that the integral-scale Reynolds number $Re_L = W_{f,rms}L/\nu$ changes from 34 to 510 as the stirring frequency increases.

The Kolmogorov dissipation length scale $\eta \approx (\nu^3/\epsilon)^{1/4}$ can be evaluated using the expression for the dissipation rate $\epsilon \approx W_f^3/L$ [32,33]. The dissipation length scale decreases monotonically from $\eta \approx 1$ mm to $\eta \approx 0.2$ mm as the turbulence intensity increases. It follows that the size of the settling particles ranges between $o(1)\eta$ and $o(10)\eta$, thus being between the integral and dissipation length scales, $\eta < d_p < L$. Figure 3 shows the range of the parameter regime in terms of the particle size [Fig. 3(a)], Stokes number [Fig. 3(b)], and turbulence intensities. It is important to note that when a particle is smaller than the Kolmogorov length scale, the forces exerted on it are known (at least for the lower Reynolds number) [34]. However, when the settling particle is larger than the Kolmogorov scale, the analytical form for the fluid-particle forces is unknown. This condition is usually referred to as finite-size particles and, according to Ref. [35], complex turbulence-particle interactions can arise under such conditions.

The dissipation timescale $\tau_\eta = (\nu/\epsilon)^{1/2}$ is in the range $\tau_\eta \in [0.02\text{--}1.3]$ s while the integral timescale $\tau_L = L^{2/3}/\epsilon^{1/3}$ is in the range $\tau_L \in [0.5\text{--}8.0]$ s. It follows that the particle relaxation time τ_p calculated according to Ref. [26] (Table I) lies between the dissipation and integral timescales,

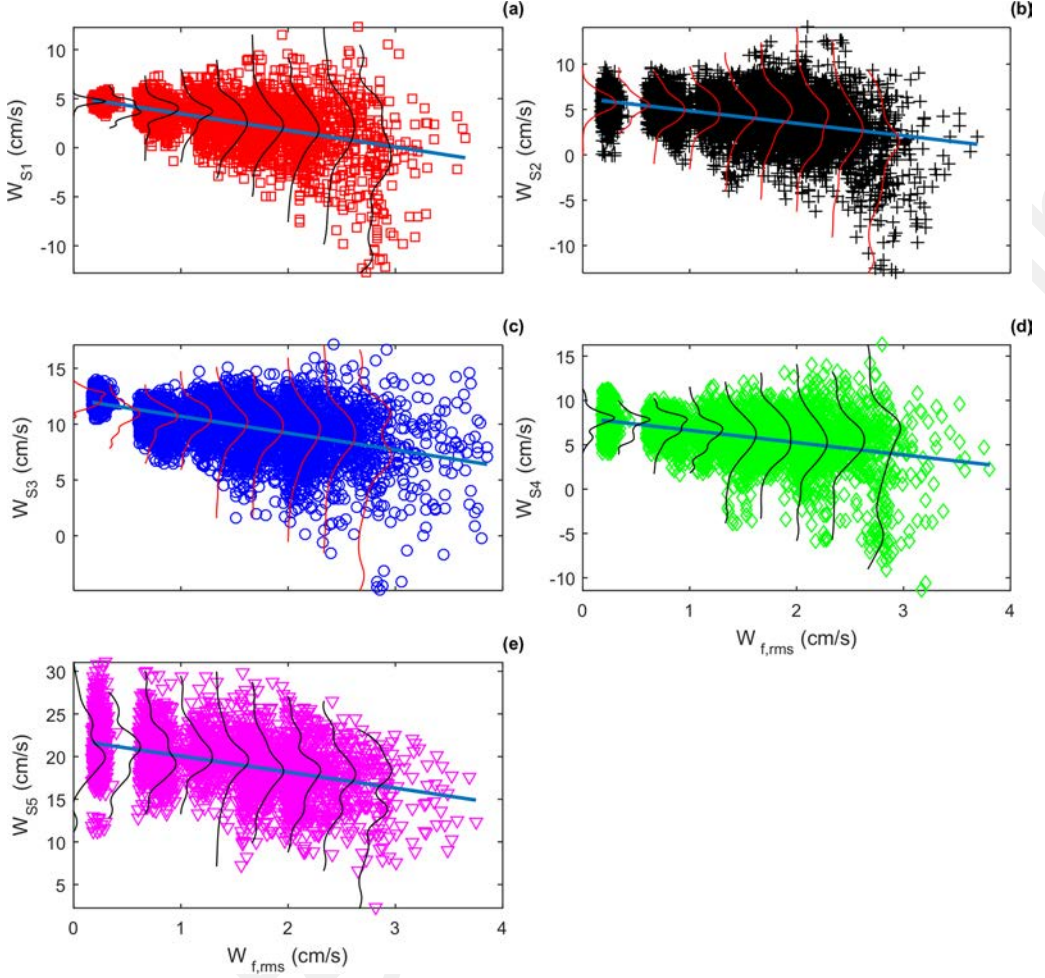


FIG. 4. Scatter plots of the instantaneous particle settling velocities as functions of the local vertical turbulence intensities $W_{f,rms}$ for particle types S1–S5. The solid blue lines correspond to the linear regressions models. Black and red lines show the probability distribution functions of W_s for intervals of $\Delta W_{f,rms} = 0.33$ cm/s from 0 to 3.00 cm/s. (a) S1 (\square), (b) S2 ($+$), (c) S3 (\circ), (d) S4 (\diamond), and (e) S5 (∇).

$\tau_\eta < \tau_p < \tau_L$, for high turbulent intensities, while for very low ones the particle relaxation time is shorter than the dissipation timescale, $\tau_p < \tau_\eta < \tau_L$.

The particle Stokes number, defined as the ratio between the particle relaxation time and the Kolmogorov timescale, $St = \tau_p/\tau_\eta$, then varies between 0.04 and 7.6 (Fig. 3). Thus, the experimental conditions cover a range of regimes where the settling particle can be considered to be a passive scalar, perfectly following the flow ($St < 0.2$), or, where the particle is inertial and is less affected by the ambient turbulence ($St > 0.2$) [35].

It is important to note that in the present experiments the turbulence must be characterized as being relatively weak since the separation of scales is small, $L/\eta = o(10)$, and the Reynolds number is low, $Re_L = o(100)$.

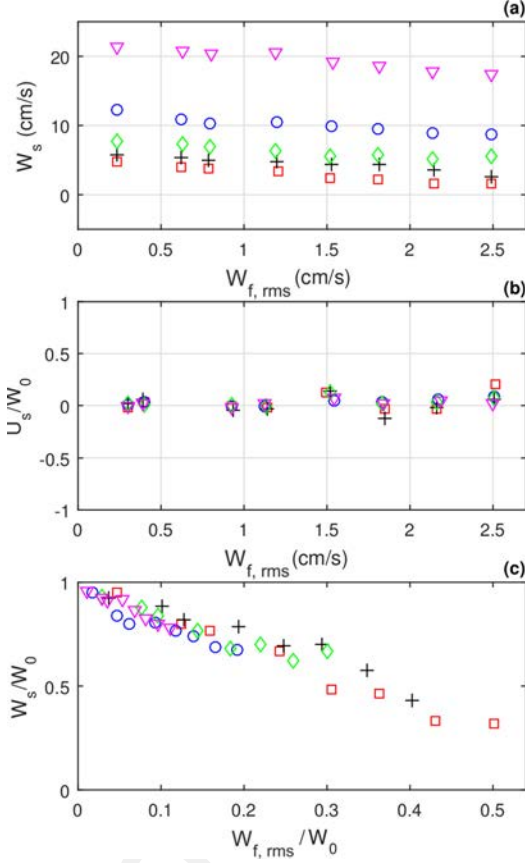


FIG. 5. Particle velocity data averaged within eight levels of turbulence intensity with a step of $\Delta W_{f,rms} = 0.33$ cm/s. (a) Particle settling velocity as a function of the vertical turbulence intensity. (b) Particle horizontal velocity as a function of the vertical turbulence intensity. (c) Particle settling velocity as a function of the vertical turbulence intensity normalized by the still-water settling velocity. S1 (\square), S2 (+), S3 (\circ), S4 (\diamond), and S5 (∇).

B. Settling velocities

Figures 4(a)–4(e) present the measured vertical instantaneous particle settling velocities for all five stirring frequencies plotted against the local vertical intensity of the ambient turbulence for the different particle types, respectively. (Note that the gap in the data at $W_{f,rms} = 0.5$ cm/s is connected to the fact that even though the measurements were done at equally spaced stirring frequencies, the standard deviation of the measured turbulent velocities is lower for lower stirring frequencies.) Note that as was mentioned before, each instantaneous particle velocity was corrected for the mean circulation in the tank by subtracting the local time-averaged velocity. The solid lines show the linear trend of the data sets. It is clear from these plots that the particle settling velocities decrease with increasing turbulence intensity for every particle type. At the same time, the standard deviation of the distribution of particle settling velocities increases with increasing turbulence intensity, at least for particle types S1–S4.

In order to quantify the observed tendencies, the turbulence intensity $W_{f,rms}$ is divided into eight intervals of $\Delta W_{f,rms} = 0.33$ cm/s, from 0 to 2.67 cm/s (beyond this value there is not enough data for statistical convergence). The particle velocities (U_s, W_s) and the associated turbulence intensities ($U_{f,rms}, W_{f,rms}$) are then averaged over each interval. Figure 5(a) shows these averaged

values against the particle settling velocity W_s . This figure should be interpreted as the average settling velocity which a particle has when it falls through a region for which the Eulerian turbulent velocity is within the interval $W_{f,rms} \pm \Delta W_{f,rms}/2$. It is clear that for these averaged values the settling velocity reduction with increasing turbulent intensity is still preserved. One must keep in mind that W_s is defined in the laboratory frame of reference which differs from the slip velocity defined in the moving frame of reference (e.g., Ref. [21]).

The average horizontal velocity of a settling particle in a turbulence column should ideally be zero. This fact allows one to verify whether the effect of the mean currents was successfully accounted for. Thus, Fig. 5(b) presents the corrected horizontal particle velocity U_s . It is clear that it does deviate from zero. However, its value is less than 10% of W_0 except for S1 at the highest turbulence intensity for which it is less than 20% of W_0 . This residual velocity is also one order of magnitude lower than the typical velocity scale of the mean flow. It is concluded that the current methodology is thus sufficient.

From Fig. 5(a) it is clear that the retardation tendency is observed for all particle types. However, it is desirable to derive a unique relationship that would describe this behavior independently of the particle properties. To this end, Fig. 5(c) presents a normalization which allows one to collapse all the data despite a relatively wide range of the particle properties. Both the particle settling velocities and the turbulence intensities are normalized by the still-water particle settling velocity. This suggests that the relation $W_s/W_0 = f(W_{f,rms}/W_0)$ could be an appropriate formalism to predict the turbulence-induced settling retardation when $\rho_p \gtrsim \rho_f$ and $Re_p^0 \gg 1$. In the next section, an analytical approach is taken to investigate the physical basis of this formulation.

Given that the sampling frequency of the settling measurements is constant, one might suspect that the present methodology to determine W_s introduces a sampling bias because low-velocity events are oversampled compared with high-velocity ones. However, the computation of the average velocity from a given number of samples must be weighted by the time a particle spends having this given velocity. Consider defining the average velocity of a cyclist going half of the distance $L/2$ uphill and half of the distance $L/2$ downhill with respective velocities of V_1 and V_2 . The average speed of the cyclist is not $(V_1 + V_2)/2$ (which would be averaging by weighting over the distance traveled), but rather it should be $(V_1 T_1 + V_2 T_2)/(T_1 + T_2)$, where T_1 and T_2 are the respective times the cyclist went uphill and downhill, which is the time-weighted average. Thus, the apparent biasing of oversampling the slow-moving regions is exactly what one must do to give more weight to the regions in which the particle spends more time, and consequently, to obtain the average value which approaches the true average as the number of samples increases.

Figures 6(a) and 6(b) present the standard deviation of the horizontal and vertical particle velocities, $U_{s,rms}$ and $W_{s,rms}$, respectively, plotted against the horizontal and vertical standard deviation of the fluid velocity, $U_{f,rms}$ and $W_{f,rms}$. Note that in order to eliminate the contribution of the particles' polydispersity, the standard deviation of the particle velocity in still water, $U_{0,rms}$ and $W_{0,rms}$ (Table I), was subtracted from $U_{s,rms}$ and $W_{s,rms}$, respectively. The straight lines in Figs. 6(a) and 6(b) correspond to the equations $U_{s,rms} - U_{0,rms} = U_{f,rms}$ and $W_{s,rms} - W_{0,rms} = W_{f,rms}$, respectively. It can be seen that the standard deviation of the particle velocities are close to that of the fluid for all the particles types except for the heaviest one, S5, for which the particle velocity fluctuations are lower. It is interesting to note that even though S5 shows such a different behavior in Fig. 6, it still follows the same trend of turbulence-induced retardation in Fig. 5(c). This suggests that the proposed scaling accounts for the differences in the particle-turbulence interaction, at least in the present regime. One can further observe that $U_{s,rms} > U_{f,rms}$ and $W_{s,rms} > W_{f,rms}$ for S1, indicating that these particles oversample more energetic turbulent regions as was suggested in Refs. [11,36,37].

It is important to note here that the flow measurements were performed independently of the particle settling measurements. Simultaneous measurements as in Ref. [21] are undoubtedly also of interest but only provide flow measurements in the vicinity of a settling particle (given modern measurement capabilities). Yet, even with perfectly resolved measurements, if a particle follows a preferential path, the measured turbulence statistics around the falling particle will be biased

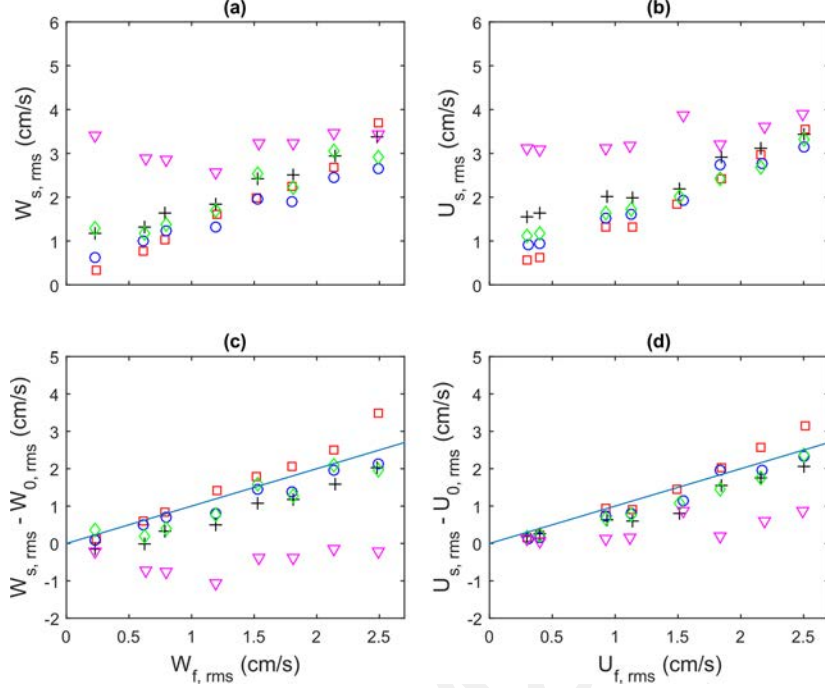


FIG. 6. (a) rms of the vertical particle velocity $W_{s,rms}$ and (b) rms of the horizontal particle velocity $U_{s,rms}$ as functions of the corresponding local turbulent velocities. $W_{0,rms}$ and $U_{0,rms}$ are the rms of the vertical and horizontal particle velocities in still water. The solid lines correspond to the equations $W_{s,rms} - W_{0,rms} = W_{f,rms}$ and $U_{s,rms} - U_{0,rms} = U_{f,rms}$. S1 (\square), S2 ($+$), S3 (\circ), S4 (\diamond), and S5 (∇).

towards the statistics in that path. Also, in practice the Eulerian background turbulence is the known characteristic and therefore relating the effective particle settling velocity to the independent background turbulence is considered to be more appropriate here.

IV. SCALING ANALYSIS FOR SETTLING RETARDATION

On the four types of particle-turbulence interaction mechanisms, fast-tracking, vortex trapping, loitering, and nonlinear drag effect (see Sec. I), a few facts are known. The fast-tracking effect is common for particles much heavier than the fluid, $\rho_p \gg \rho_f$ [9]. The vortex trapping mainly occurs for large turbulence intensities, $W_{f,rms} > W_0$ [12]. In the experiments conducted in this work the turbulence is relatively weak ($W_{f,rms}/W_0 < 0.5$), the particles are slightly denser than the fluid ($\rho_p \gtrsim \rho_f$), and their size and relaxation timescale mostly correspond to the inertial subrange of turbulence ($\eta < d_p < L$ and $\tau_\eta < \tau_p < \tau_L$) (even though for the given Reynolds numbers the separation of scales is not large enough for a distinct inertial subrange). It follows that the nonlinear drag and loitering effects are likely the main mechanisms influencing particle settling in the present conditions. Hence, for both effects a simple analytical model is proposed to infer the observed scaling law for settling retardation.

Before developing the scaling arguments, the minimum fluid-particle force model needs to be selected. According to the review of Michaelides [38], the average particle velocity can be reasonably well predicted for solid particles having relative density of order 1–2 by the steady drag force only. According to the author, the relative importance of history force on particle dispersion is lower than 8% for fluid velocity frequencies less than 17 Hz. In the present experimental conditions,

the velocity frequencies never exceed 9 Hz, which supports the assumption of neglecting this force in the scaling analysis.

A. Nonlinear drag

For a high particulate Reynolds number ($\text{Re}_p^0 \gg 1$) the drag force exerted on a particle by the flow is proportional to the relative velocity squared, $\vec{F}_D = 0.5\rho A\alpha'_D\vec{V}^2$, where ρ is the density of the fluid, A is the surface area, and α'_D is the drag coefficient which may slightly depend on \vec{V} [8]. For the sake of simplicity, assume $\alpha_D = 0.5\rho A\alpha'_D$. Then, it can be written that $\vec{F}_D = \alpha_D\vec{V}^2$. Now, consider a case of an idealized interaction between an infinitely inertial particle and homogeneous turbulence with only one component of velocity fluctuations ΔW . Then, the relative velocity of the particle to the fluid is $\vec{V}(t) = W_0 \pm \Delta W$, with equal time allocated for positive and negative fluctuations, i.e., the temporal average of \vec{V} is W_0 and the associated standard deviation is ΔW . If one assumes that α_D is constant over $[W_0 - \Delta W; W_0 + \Delta W]$, the instantaneous drag force becomes $F_D^\pm = \alpha_D(W_0 \pm \Delta W)^2$. As negative and positive fluctuations are considered to be equally distributed in time, it can be shown that the time-averaged drag force is $F_D^{\text{NLD}} = \alpha_D(W_0^2 + \Delta W^2)$. Taking W_0 out of the parentheses results in the following expression for the drag force induced by the velocity fluctuations through the nonlinear drag effect,

$$F_D^{\text{NLD}} = \alpha_D \left(1 + \frac{\Delta W^2}{W_0^2} \right) W_0^2. \quad (3)$$

An effective drag coefficient α_D^{NLD} can then be written as

$$\alpha_D^{\text{NLD}} = \alpha_D \left(1 + \frac{\Delta W^2}{W_0^2} \right). \quad (4)$$

Both in the absence and in the presence of turbulence, the settling particle, given that it reached the statistical steady state, is in equilibrium between two forces, the drag force and the gravity force. Hence, in still water one can write that

$$m'_p g = F_D^0 = \alpha_D W_0^2, \quad (5)$$

where $m'_p g$ is the immersed weight of the particle [7], and in a turbulent environment it leads to

$$m'_p g = F_D^{\text{NLD}} = \alpha_D^{\text{NLD}} W_s^{\text{NLD}2}, \quad (6)$$

where W_s^{NLD} is the particle settling velocity taking into account the nonlinear drag effect. That is, the drag force exerted on the particle is the same, while the drag coefficient and the settling velocity vary. Dividing (6) by (5) results in the following expression,

$$\frac{W_s^{\text{NLD}}}{W_0} = \sqrt{\frac{\alpha_D}{\alpha_D^{\text{NLD}}}}. \quad (7)$$

Substituting (4) into (7), an estimate of the turbulence-induced settling retardation due to the nonlinear drag effect is obtained,

$$\frac{W_s^{\text{NLD}}}{W_0} = \frac{1}{\sqrt{1 + \frac{\Delta W^2}{W_0^2}}}. \quad (8)$$

Notably, this result is consistent with the scaling law obtained experimentally, i.e., $W_s/W_0 = f(W_{f,\text{rms}}/W_0)$. That is, it does not depend on the particle properties, except through W_0 since the drag coefficient was canceled out during the derivation.

The main assumption made here is that α_D is constant over $[W \pm \Delta W]$. This is valid when $\text{Re}_p^0 \geq o(10^3)$ for any ΔW , and can be considered reasonable when $\text{Re}_p^0 = o(10^2)$ for relatively small ΔW [8].

B. Loitering

A settling particle crosses regions of upward velocity fluctuations more slowly than regions of downward velocity fluctuations assuming that a particle has sufficiently low inertia and quickly adapts its velocity to that of the surrounding fluid [12]. Consequently, while traveling a certain distance, a particle spends on average a longer time in upward velocity regions than in downward ones, provided that both are uniformly distributed in space [18]. This asymmetry implies that even in statistically homogeneous isotropic turbulence the mean fluid velocity “seen” (or sampled) by the particle $W_{f/p}$ is not zero and is directed upward. It can also be interpreted as a particle settling on average in a fluid frame of reference moving upward with a velocity $W_{f/p}$. Thus, the mean particle fall velocity in the frame of reference of an external observer is reduced. (Recall the cyclist who spends a longer time traveling a given distance uphill than downhill, resulting in a mean velocity lower than the arithmetic mean of the uphill and downhill velocities.) This phenomenon is called the loitering effect. A formalization of its influence on the particle settling is provided in the following.

Consider a very simple model: a steady turbulent flow whose regions of negative and positive velocity fluctuations ($\pm\Delta W$) are arranged in a chessboard pattern. If the typical spatial extent L' of the boxes is uniform, the spatial average of the fluid velocity is zero and the spatial standard deviation is ΔW . Following Ref. [11], it is further assumed that the particle settles in one dimension, crossing alternatively the regions of positive and negative fluctuations. Two extreme cases are then considered: infinite- and zero-inertia particles.

A particle with infinite inertia falls without adapting its velocity to that of the surrounding fluid. The time-averaged fluid velocity “seen” by the particle $W_{f/p}$ is then zero, resulting in no loitering effect. Note that in this case, the relative velocity between the particle and the fluid is $\vec{V}(t) = W_0 \pm \Delta W$, with identical time fractions for $\vec{V} = W_0 + \Delta W$ and $\vec{V} = W_0 - \Delta W$. This case corresponds to the idealized interaction model previously introduced to derive the nonlinear drag formulation (8).

In the case of a zero-inertia particle, the particle instantaneously adapts its velocity to the velocity of the surrounding fluid [26]. Hence, the relative velocity between the fluid and the particle is always that of the still-water settling, $\vec{V} = W_0$. The particle absolute velocity is then $W_s^+ = W_0 + \Delta W$ in the upward velocity regions, and $W_s^- = W_0 - \Delta W$ in the downward ones. The associated time periods spent in these regions are $\Delta T^+ = L'/W_s^+$ and $\Delta T^- = L'/W_s^-$, respectively, and the time-averaged settling velocity taking into account the loitering effect W_s^L is

$$W_s^L = \frac{\Delta T^- W_s^- + \Delta T^+ W_s^+}{\Delta T^+ + \Delta T^-}. \quad (9)$$

Substituting expressions for ΔT^\pm and W_s^\pm into this equation leads to an estimate of particle settling retardation due to the loitering effect,

$$\frac{W_s^L}{W_0} = 1 - \frac{\Delta W^2}{W_0^2}. \quad (10)$$

This equation can also be expressed as $W_s^L = W_0 + W_{f/p}$, where $W_{f/p} = -W_{f,\text{rms}}^2/W_0$ is the time-averaged fluid velocity sampled or “seen” by the particle. The loitering effect can then be interpreted as a sampling bias inducing an upward velocity of the fluid frame in which the particle settles.

It is remarkable that both results, for the nonlinear drag [Eq. (8)] and loitering [Eq. (10)] effects, predict turbulence-induced settling retardation consistent with the scaling law obtained experimentally, i.e., $W_s/W_0 = f(W_{f,\text{rms}}/W_0)$. This is, assuming $\Delta W = W_{f,\text{rms}}$ (a reasonable approximation if W'_f has a symmetric distribution). Given that the flow under consideration is forced by symmetric grids, even at the largest scales the symmetry is expected to be preserved. The distributions of W'_f are also shown in Fig. 4.

V. CONCLUSIONS

The effect of ambient turbulence on the settling of solid particles was investigated herein. Experiments were conducted in a turbulence column with oscillating grids which reproduced quasi-isotropic homogeneous turbulence in the measurement region to the degree of the turbulent correlation coefficient being less than 0.1. Weak but unavoidable mean currents were subtracted from the measured particle instantaneous velocities. Five different particle types having a density ratio of order unity ($\rho_p/\rho_f = 1.1\text{--}2.6$) were tested. The particle size ratio d_p/η varied between $o(1)$ and $o(10)$ and the Stokes number St_η , based on the Kolmogorov timescale, was of order unity. The particulate Reynolds number Re_p^0 varies between 75 and 981. This means that in this regime inertial effects are non-negligible both from the fluid and particle standpoint. Also, that the present experiments can be considered to be in the regime of finite-size particles [35] where an analytical form for the fluid-particle forces is unknown.

The results can be summarized as follows:

(1) Retardation of particle settling was observed for every particle type; stronger retardation corresponded to higher turbulence intensity. Scaling both the effective particle settling velocity W_s and the turbulence intensity $W_{f,\text{rms}}$ by the still-water particle settling velocity W_0 allowed us to obtain a unique relationship between the settling retardation and the dimensionless turbulence intensity. Thus, in the parameter range investigated herein, the settling retardation does not depend on the particle properties (size, shape, density) except through W_0 and can be described with a relationship $W_s/W_0 = f(W_{f,\text{rms}}/W_0)$.

(2) The independence of the turbulence-induced settling retardation from the particle properties may appear counterintuitive since the drag intrinsically depends on the particle properties through the drag coefficient and the choice of the model thereof. However, the results of the analytical derivation for the nonlinear drag [Eq. (8)] and loitering effects [Eq. (10)] confirm this finding. The drag coefficient cancels out and the settling retardation only depends on turbulence intensity and the still-water settling velocity.

(3) Both analytical formulations also predict turbulence-induced settling retardation and are consistent with the scaling law obtained experimentally, i.e., $W_s/W_0 = f(W_{f,\text{rms}}/W_0)$. It should be highlighted that neither one suggests that W_s/W_0 is a linear function of $W_{f,\text{rms}}/W_0$, while the experimental results [Fig. 5(c)] appear almost linear. This is not completely unexpected as settling retardation is probably a combination of these two effects and maybe other effects are important as well. For example, as it was noted before, for lower turbulence intensities a particle is expected to be able to adapt its velocity to the velocity of the fluid, increasing the relevance of the loitering effect. For higher turbulence intensity a particle may not have enough time to adapt its velocity to the passing eddies, thus increasing the relevance of the nonlinear drag effect. The contribution of each factor may also be a nonlinear function of the turbulence intensity.

(4) We hypothesize that the fact that the particles considered are always greater than the Kolmogorov length scale plays a key role in the observed settling retardation. Indeed, scaling laws for loitering and nonlinear drag effects alone cannot explain quantitatively the observations and finite-size effect is the only process which is occurring in all the experiments unlike the particle's inertial effect (a Stokes number sometimes lower than 0.2). However, in order to exhaustively answer this question, fully resolved direct numerical simulations at the particle scale shall be performed.

To conclude, a unique set of well-controlled settling experiments has been conducted showing settling retardation for a range of flow and particle properties, Re_p^0 varying between 75 and 981 and Re_L in the range of 34–510. A scaling law was obtained to quantify the effect of turbulence on particle settling in the given regime. Analytical formulations were obtained which showed that this scaling law has a physical basis. This scaling will potentially help to further analyze and compare different sets of experimental and numerical data. Direct numerical simulation at the particle scale is probably the best methodology to address this problem and disentangle the various effects mentioned in this work as well as other physical mechanisms.

- [1] N. L. Coleman, Flume studies of the sediment transfer coefficient, *Water Resour. Res.* **6**, 801 (1970).
- [2] E. Doroodchi, G. M. Evans, M. P. Schwarz, G. L. Lane, N. Shah, and A. Nguyen, Influence of turbulence intensity on particle drag coefficients, *Chem. Eng. J.* **135**, 129 (2008).
- [3] A. Ansmann, F. Rittmeister, R. Engelmann, S. Basart, A. Benedetti, C. Spyrou, A. Skupin, H. Baars, P. Seifert, F. Senf, and T. Kanitz, Profiling of Saharan dust from the Caribbean to West Africa, Part 2: Shipborne lidar measurements versus forecasts, *Atmos. Chem. Phys. Discuss.* **1** (2017).
- [4] M. R. Maxey, The gravitational settling of aerosol particles in homogeneous turbulence and random flow fields, *J. Fluid Mech.* **174**, 441 (1987).
- [5] E. A. Toorman, Vertical mixing in the fully developed turbulent layer of sediment-laden open-channel flow, *J. Hydraul. Eng.* **134**, 1225 (2008).
- [6] M. W. Schmeeckle, Numerical simulation of turbulence and sediment transport of medium sand, *J. Geophys. Res.: Earth Surf.* **119**, 1240 (2014).
- [7] P. Nielsen, On the motion of suspended sand particles, *J. Geophys. Res.: Oceans* **89**, 616 (1984).
- [8] P. A. Hwang, Fall velocity of particles in oscillating flow, *J. Hydraul. Eng.* **111**, 485 (1985).
- [9] L.-P. Wang and M. R. Maxey, Settling velocity and concentration distribution of heavy particles in homogeneous isotropic turbulence, *J. Fluid Mech.* **256**, 27 (1993).
- [10] K. Kawanisi and R. Shiozaki, Turbulent effects on the settling velocity of suspended sediment, *J. Hydraul. Eng.* **134**, 261 (2008).
- [11] G. H. Good, P. J. Ireland, G. P. Bewley, E. Bodenschatz, L. R. Collins, and Z. Warhaft, Settling regimes of inertial particles in isotropic turbulence, *J. Fluid Mech.* **759**, R3 (2014).
- [12] P. Nielsen, Turbulence effects on the settling of suspended particles, *J. Sediment. Petrol.* **63**, 835 (1993).
- [13] H W Ho, Fall velocity of a sphere in an oscillating fluid, Ph.D. thesis, University of Iowa, 1964.
- [14] R. Mei, Effect of turbulence on the particle settling velocity in the nonlinear drag range, *Int. J. Multiphase Flow* **20**, 273 (1994).
- [15] J. E. Stout, S. P. Arya, and E. L. Genikhovich, The effect of nonlinear drag on the motion and settling velocity of heavy particles, *J. Atmos. Sci.* **52**, 3836 (1995).
- [16] C. Y. Yang and U. Lei, The role of the turbulent scales in the settling velocity of heavy particles in homogeneous isotropic turbulence, *J. Fluid Mech.* **371**, 179 (1998).
- [17] J. Bec, H. Homann, and S. S. Ray, Gravity-Driven Enhancement of Heavy Particle Clustering in Turbulent Flow, *Phys. Rev. Lett.* **112**, 184501 (2014).
- [18] B. Rosa, H. Parishani, O. Ayala, and L.-P. Wang, Settling velocity of small inertial particles in homogeneous isotropic turbulence from high-resolution DNS, *Int. J. Multiphase Flow* **83**, 217 (2016).
- [19] P. J. Ireland, A. D. Bragg, and L. R. Collins, The effect of Reynolds number on inertial particle dynamics in isotropic turbulence. Part 2. Simulations with gravitational effects, *J. Fluid Mech.* **796**, 659 (2016).
- [20] S. P. Murray, Settling velocities and vertical diffusion of particles in turbulent water, *J. Geophys. Res.* **75**, 1647 (1970).
- [21] Q. Zhou and N.-S. Cheng, Experimental investigation of single particle settling in turbulence generated by oscillating grid, *Chem. Eng. J.* **149**, 289 (2009).
- [22] G. Kuehn and G. H. Jirka, Fine sediment behavior in open channel turbulence: An experimental study, in *Sediment Dynamics and Pollutant Mobility in Rivers: An Interdisciplinary Approach*, edited by B. Westrich and U. Förstner (Springer, Berlin, 2007), p. 99.
- [23] B. Brunk, M. Weber-Shirk, A. Jensen, G. Jirka, and L. W. Lion, Modeling natural hydrodynamic systems with a differential-turbulence column, *J. Hydraul. Eng.* **122**, 373 (1996).
- [24] A. M. Fincham and G. R. Spedding, Low cost, high resolution DPIV for measurement of turbulent fluid flow, *Exp. Fluids* **23**, 449 (1997).
- [25] A. Fincham and G. Delerce, Advanced optimization of correlation imaging velocimetry algorithms, *Exp. Fluids* **29**, S013 (2000).
- [26] S. Balachandar, A scaling analysis for point-particle approaches to turbulent multiphase flows, *Int. J. Multiphase Flow* **35**, 801 (2009).
- [27] T. Revil-Baudard, J. Chauchat, D. Hurther, and P.-A. Barraud, Investigation of sheet-flow processes based on novel acoustic high-resolution velocity and concentration measurements, *J. Fluid Mech.* **767**, 1 (2015).

- [28] T. Revil-Baudard, J. Chauchat, D. Hurther, and O. Eiff, Turbulence modifications induced by the bed mobility in intense sediment-laden flows, *J. Fluid Mech.* **808**, 469 (2016).
- [29] A. A. Townsend, *The Structure of Turbulent Shear Flow* (Cambridge University Press, Cambridge, U.K., 1976), p. 433.
- [30] C. Manes, D. Poggi, and L. Ridolfi, Turbulent boundary layers over permeable walls: Scaling and near-wall structure, *J. Fluid Mech.* **687**, 141 (2011).
- [31] W. H. Snyder and J. L. Lumley, Some measurements of particle velocity autocorrelation functions in a turbulent flow, *J. Fluid Mech.* **48**, 41 (1971).
- [32] G. I. Taylor, Statistical theory of turbulence, *Proc. R. Soc. London, Ser. A* **151**, 444 (1935).
- [33] J. C. Vassilicos, Dissipation in turbulent flows, *Annu. Rev. Fluid Mech.* **47**, 95 (2015).
- [34] M. R. Maxey and J. J. Riley, Equation of motion for a small rigid sphere in a nonuniform flow, *Phys. Fluids* **26**, 883 (1983).
- [35] S. Balachandar and J. K. Eaton, Turbulent dispersed multiphase flow, *Annu. Rev. Fluid Mech.* **42**, 111 (2010).
- [36] L.-P. Wang and D. E. Stock, Dispersion of heavy particles by turbulent motion, *J. Atmos. Sci.* **50**, 1897 (1993).
- [37] J. P. L. C. Salazar and L. R. Collins, Inertial particle relative velocity statistics in homogeneous isotropic turbulence, *J. Fluid Mech.* **696**, 45 (2012).
- [38] E. E. Michaelides, The transient equation of motion for particles, bubbles, and droplets, *J. Fluids Eng.* **119**, 233 (1997).